Structure and function of a virally encoded fungal toxin from *Ustilago maydis*: a fungal and mammalian Ca^{2+} channel inhibitor

Fei Gu[1], Anis Khimani[2], Stanley G Rane[1], William H Flurkey[3], Robert F Bozarth[2] and Thomas J Smith[1]*

[1]Department of Biological Sciences, Purdue University, West Lafayette, IN 47907, USA, [2]Department of Life Sciences, Indiana State University, Terre Haute, IN 47809, USA and [3]Department of Chemistry, Indiana State University, Terre Haute, IN 47809, USA

Background: The P4 strain of the corn smut fungus, *Ustilago maydis*, secretes a fungal toxin, KP4, encoded by a fungal virus (UMV4) that persistently infects its cells. UMV4, unlike most other (non-fungal) viruses, does not spread to uninfected cells by release into the extracellular milieu during its normal life cycle and is thus dependent upon host survival for replication. In symbiosis with the host fungus, UMV4 encodes KP4 to kill other competitive strains of *U. maydis*, thereby promoting both host and virus survival. KP4 belongs to a family of fungal toxins and determining its structure should lead to a better understanding of the function and evolutionary origins of these toxins. Elucidation of the mechanism of toxin action could lead to new anti-fungal agents against human pathogens.

Results: We have determined the atomic structure of KP4 to 1.9 Å resolution. KP4 belongs to the α/β-sandwich family, and has a unique topology comprising a five-stranded antiparallel β-sheet with two antiparallel α-helices lying at ~45° to these strands. The structure has two left-handed βαβ cross-overs and a basic protuberance extending from the β-sheet. *In vivo* experiments demonstrated abrogation of toxin killing by Ca^{2+} and, to a lesser extent, Mg^{2+}. These results led to experiments demonstrating that the toxin specifically inhibits voltage-gated Ca^{2+} channels in mammalian cells.

Conclusions: Similarities, although somewhat limited, between KP4 and scorpion toxins led us to investigate the possibility that the toxic effects of KP4 may be mediated by inhibition of cation channels. Our results suggest that certain properties of fungal Ca^{2+} channels are homologous to those in mammalian cells. KP4 may, therefore, be a new tool for studying mammalian Ca^{2+} channels and current mammalian Ca^{2+} channel inhibitors may be useful lead compounds for new anti-fungal agents.

Structure 15 August 1995, **3**:805–814
Key words: α/β fold, Ca^{2+} channels, fungal toxin

Introduction

Several strains of *Ustilago maydis* (corn smut fungus) and *Saccharomyces cerevisiae* (yeast) have been classified as 'killer' strains by their ability to kill similar strains of fungi in culture. This killer phenotype is caused by persistent infections of the host cells by double-stranded (ds) RNA virions. These virions are unusual in that they are not expressed externally but instead are transmitted vertically through basidiospores or horizontally through anastomosis [1,2]. The multisegmented viral genome is encased by an unusual type of capsid composed of 120 copies of the envelope protein *gag* [3–6]. The structures of two of these viruses have been determined using cryo-electron microscopy and image reconstruction techniques [6]. With two identical copies of *gag* in each icosahedral asymmetric unit, these capsids were found to contradict Caspar and Klug's rules [7] for icosahedral equivalency without any topological evidence of acceptable pseudo-symmetry such as P=4. It was speculated that these viral capsids do not act as protective carapaces but rather as cytoplasmic compartments for viral genome replication [6].

Unlike most non-fungal viruses, some of these dsRNA fungal viruses have a symbiotic relationship with their host. These viruses are solely dependent upon host survival for replication, and therefore lend the host a selective advantage by encoding small toxins that are secreted by the host cell. The fungal toxins do not affect the host cell strain but do kill similar strains of fungi in that locale.

In *S. cerevisiae*, the two best-studied classes of toxins are K_1 and K_2. The members of one class are immune to the toxins of other members of the same class but sensitive to the killing action of the other class [8]. K_1 is composed of two subunits linked together via a disulfide bond [9–12]. One subunit is predicted to have a hydrophobic, α-helical secondary structure typical of membrane-spanning proteins. The other domain is hydrophilic and thought to be involved in protecting the host from toxic effects [13]. It has been proposed that the K_1 toxin first binds to the cell wall, targets secondary receptors at the cell membrane, and then either acts as a protonophore or alters existing ionophores [14–16]. Subsequent experiments demonstrated that the K_1 toxin forms ion channels in

*Corresponding author.

 ISSN 0969-2126

sensitive yeast spheroplasts and in artificial membranes [17]. In addition, a toxin from the yeast *Pichia kluyveri*, with physiological properties similar to those of *S. cerevisiae* K_1, has also been shown to have channel-forming activity in synthetic membranes [18].

In *U. maydis*, three killer toxins have been described to date — KP1, KP4 and KP6 [19–21]. KP1 and KP6 are both composed of two non-covalently linked polypeptides, each comprising ~80 amino acids. As for the yeast toxins, KP6 receptors are thought to reside in the cell wall. However, unlike the yeast toxins, both subunits of KP6 are thought to be involved in killing [22–24]. The lack of spheroplast sensitivity to KP6 suggests that no secondary receptor exists on the cell membrane [23]. Preliminary evidence suggests that KP6, using both subunits, may also form channels in planar phospholipid membranes [25], and that these subunits form mostly β-sheets in the presence of phospholipids [26].

KP4 is unlike other previously described toxins from killer strains of *S. cerevisiae* (K1, K2 and KT28 [8]) and *U. maydis* (KP1 and KP6 [19–21]). Whereas these other toxins are composed of two polypeptides and are believed to form ion channels in the cell membrane [14–16], KP4 is a single polypeptide for which the mechanism of action is undefined [21]. Another difference is that the yeast toxins are acidic proteins [27], the other *U. maydis* toxins are neutral [28], but KP4 is very basic with an isoelectric point (pI) greater than 9 [29]. No atomic structure is available for any of these toxins.

Here we report the atomic structure of KP4 at 1.9 Å resolution. The structure was determined by the isomorphous replacement method and phase improvement using anomalous dispersion, solvent flattening and real-space averaging techniques. KP4 belongs to the α/β-sandwich family of proteins and contains an approximate internal dyad axis. Similarities between KP4 and scorpion toxins led to experiments demonstrating the abrogation of toxin effects by Ca^{2+} and Mg^{2+} but not by Na^+ or K^+. These results suggest that KP4 acts at the cell membrane by closing channels for divalent cations. This was further substantiated by the surprising result that KP4 blocks voltage-gated Ca^{2+} channels in mammalian cells.

Results and discussion

Structure determination

The previously reported crystal form of KP4 was $P6_{1(5)}22$, contained two copies of KP4 per asymmetric unit, and diffracted X-rays to ~2.8 Å resolution [30]. Under very different conditions (see the Materials and methods section for details), KP4 was crystallized in another crystal form. This new crystal form belongs to the $P2_1$ space group, diffracts X-rays to >1.7 Å resolution (Table 1), and contains two copies of toxin per asymmetric unit. The phases were determined from a single derivative and were improved using solvent flattening, twofold real-space averaging, and anomalous dispersion from the heavy atom. All 105 residues in each copy of KP4 were unambiguously assigned. The two copies of KP4 have been refined independently and include a total of 109 water molecules in the asymmetric unit. The current model has been refined to an R-factor of 18.6% (R_{free}=23.7%) using all data between 6.0 Å and 1.9 Å resolution. A typical example of the electron density is shown in Figure 1. The root mean square (rms) deviation in Cα positions between the two copies of KP4 in the asymmetric unit is 0.249 Å.

Table 1. Crystallographic data statistics.

Parameters	Native	$KAu(CN)_2$
Structure determination		
Heavy-atom soaking time (days)	–	9
Data collection device	R-axis	R-axis
Temperature (°C)	4	4
Resolution (Å)	1.7	2.5
Data completeness (%)	81.9	90.1
Unique reflections	15905	5571
Redundancy	3.42	4.04
R_{sym}* (%)	5.2	8.5
Molecules/asym. unit	2	
R_{iso}† (%)		13.4
No. of heavy atom sites		4
R_{Cullis}‡ (centric)		0.61
R_{Cullis} (acentric)		0.75
R_{Cullis} anomalous		0.91 (0.96)
Phasing power		1.36 (0.72)
Structure refinement		
Resolution (Å)	6.0–1.9	
R_{cryst}§ (%)	18.6	
R_{free}# (%)	23.7	
No. of non-hydrogen atoms	1530	
No. of water molecules	109	
Rms bond length (Å)	0.0189	
Rms bond angle (°)	1.95	
G factor [54]	0.3	
Ramachandran plot outliers	0	

*R_{sym} is the unweighted R-value on I between symmetry-related observations. †$R_{iso}=\Sigma(|F_{ph}|-|F_p|)/\Sigma|F_p|$. ‡$R_{Cullis}=\Sigma[|F_h|-(|F_{ph}|-|F_p|)]/\Sigma|F_h|$ for centric and acentric reflections. R_{Cullis} anomalous is calculated using anomalous data. §$R_{cryst}=\Sigma|F_{obs}-F_{calc}|/\Sigma|F_{obs}|$. #$R_{free}$ was calculated using 10% of the data separated from the rest of the reflections before a full cycle of simulated annealing in X-PLOR [54].

Details of the KP4 structure

Interactions between the two copies of KP4 in the asymmetric unit are mediated by polar and charged residues. A number of these are indirect, involving hydrogen bonds via water molecules in the intermolecular interface. This dimer structure is unlikely to have biological significance as cross-linking, size-exclusion chromatography and NMR spectroscopy studies (data not shown) all suggest that the toxin is monomeric in solution.

KP4 belongs to the α/β-sandwich family of proteins and has a single split βαβ motif (for a review, see [31]). The toxin has a total of seven β-strands (β1–β7) and three α-helices (α1–α3; Fig. 2). This contradicts previous circular dichroism spectroscopy results and secondary-structure

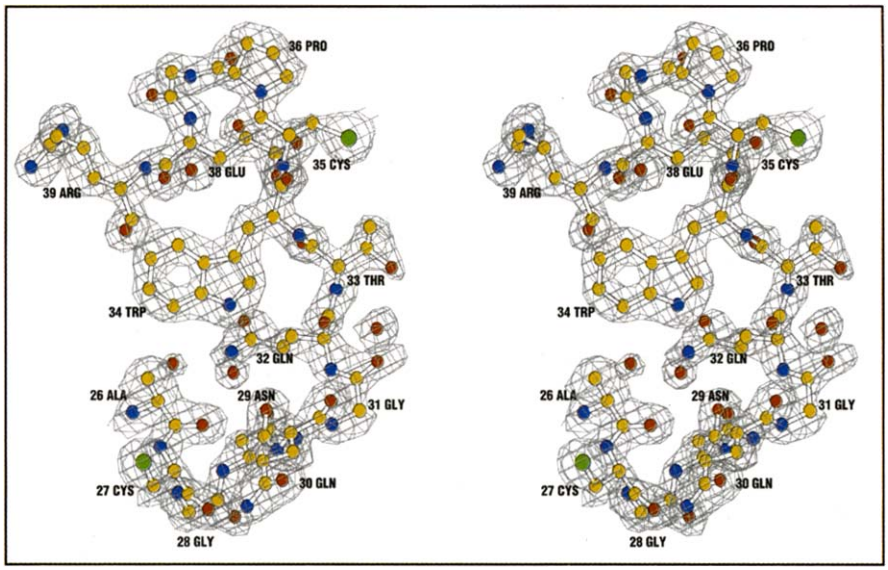

Fig. 1. Typical example of the $2F_o–F_c$ electron density calculated to 1.9 Å resolution using model phases. The electron density, shown in gray, is contoured at 1σ. The atomic model (residues 26–39) is represented by a ball-and-stick image where the oxygens are red, carbons yellow, sulfurs green, and nitrogens blue. For clarity, the program MolView [55] was used to trim away electron density >2.0 Å away from any atom within this loop. It should be noted, however, that no unassigned density was removed during this process.

predictions which suggested that KP4 had very little helical character [30]. The major secondary-structure elements are a five-stranded antiparallel β-sheet (β1, β3, β4, β6 and β7) and a pair of antiparallel α-helices (α2 and α3) lying at an angle of approximately 45° to the strands in the β-sheet.

The first β-strand, β1, is only two residues long and is terminated by the disulfide bond between residues 5 and 78. A short, four-residue helix (α1) lies between β1 and the first main helix, α2. This helix contains a disulfide bond connecting it to strand β6 (residues 11 and 81, respectively). Helix α2 is 10 residues long and transverses the β-sheet via a left-handed βαβ connection and is joined by a disulfide bond to the last α-helix, α3 (residues 27 and 67, respectively). The C terminus of α2 is stabilized by the short strand, β2, and then by a disulfide bond between residues 35 and 60. The β3–β4 turn forms a very large protuberance at the edge of the sheet that is stabilized by the C terminus via β-sheet hydrogen bonds and a disulfide bond (residues 44 and 105). Helix α3 transverses back across the β-sheet towards the N terminus and lies antiparallel to α2. As with the α2 helix, α3 is part of a left-handed βαβ cross-over. In a similar way to the β3–β4 turn, the β6–β7 turn forms a large extension from the β-sheet, but it is not as extended as the β3–β4 turn, nor is it stabilized by a disulfide bond. Whereas the two left-handed βαβ cross-overs are unusual, it is not clear whether they have a particular functional role in KP4.

The KP4 motif is very similar to many of the other α/β proteins, but with some important differences. Domain 2 of the biotin holoenzyme synthetase is classified as having a similar topology [31]. One of the major differences between this domain and KP4 is that the biotin holoenzyme domain is significantly larger, having two additional β-strands in the β-sheet. If the connectivity is ignored and only some of the secondary elements of KP4 are used for comparison, similarities can easily be observed with many of the α/β proteins, such as scorpion toxin [32,33], protein G [34,35] and the ribonucleases [36–40]. However, as the members of the α/β-sandwich family are known for having very similar structures but very different functions, the toxin mechanism cannot be deduced from an analysis of the protein topology alone.

KP4 is very stable, resisting the effects of organic solvents, elevated temperatures and proteolytic enzymes (data not shown). The reasons for this stability are clear from the structure. Almost all of the hydrophobic residues are buried between the amphipathic helices and a hydrophobic patch on the β-sheet. Both the C and N termini are affixed to the β-sheet via disulfide bonds. Disulfide bonds also connect the ends of the helices to the β-sheet and to each other. Finally, the protein is stabilized by having almost all of its residues involved in the various secondary structural elements. Because of these stabilizing interactions, it seems unlikely that the toxin is capable of undergoing the kinds of conformational changes required to expose the amphipathic helices and form ion channels.

A pseudo-dyad axis lies between the two main α-helices and perpendicular to the β-sheet. Rotation about this axis yields good agreement between the N-terminal and C-terminal halves of the protein (an rms difference of 2.2 Å between Cα positions when 59 of the 105 corresponding Cαs are compared using 'O' [41]; Fig. 3). This symmetrical relationship suggests that the toxin may have arisen by gene duplication. However, because of the lack of sequence conservation between the two halves of the protein, any such gene duplication is probably not a recent evolutionary event. It is tempting to speculate that this internal symmetry may somehow be related to toxin recognition and attack of target cells. When the two halves of the toxin are superimposed, one of the largest differences is found between the β3–β4 turn and the rotated β6–β7 turn. These differences may be due to the fact that the C terminus interacts extensively with the

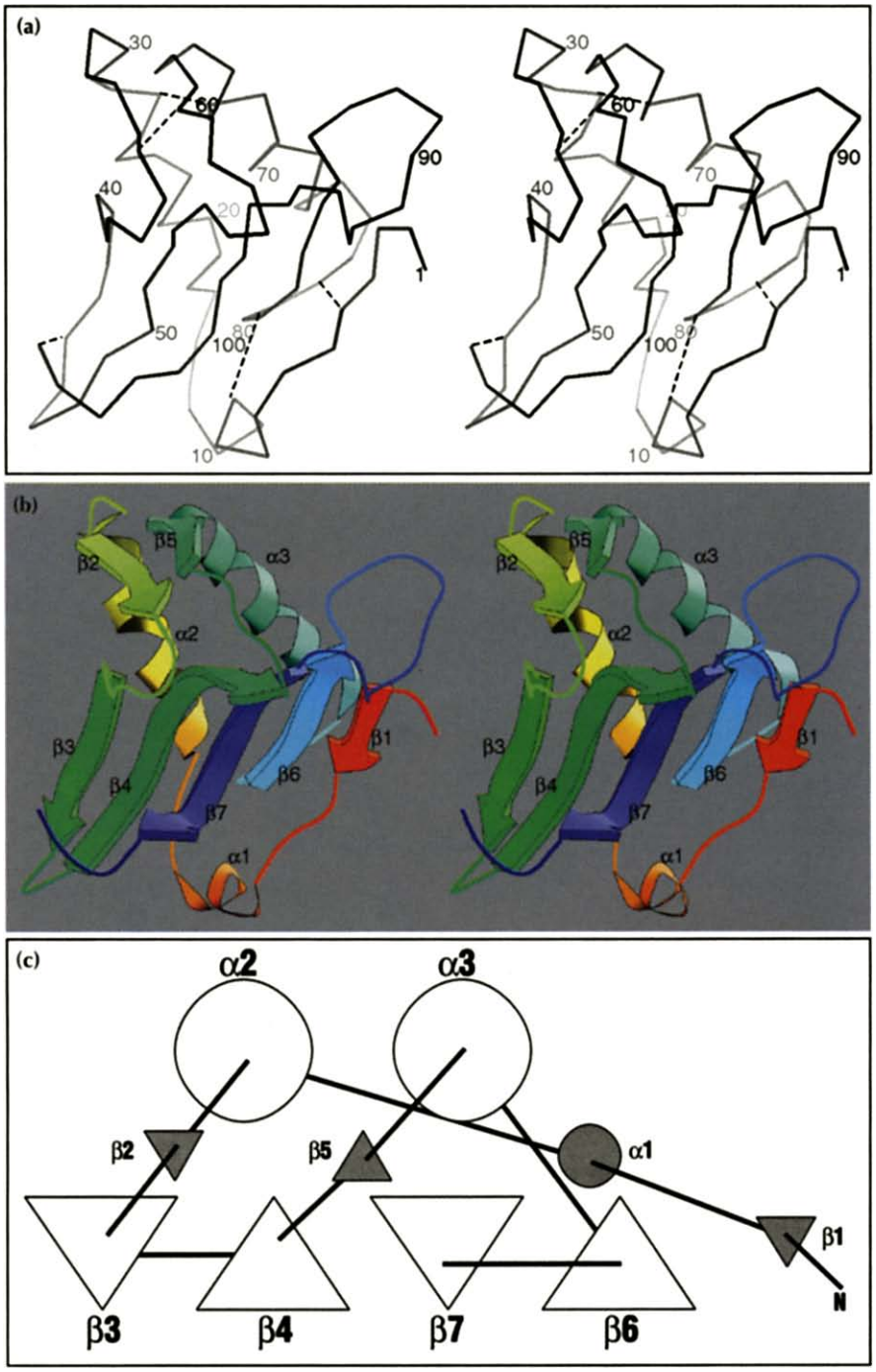

Fig. 2. Topology and structure of KP4. **(a)** Stereo, depth-cued, Cα backbone of KP4 with every tenth residue labeled. Disulfide connections are represented by dashed lines. **(b)** Ribbon drawing of KP4 where the polypeptide chain follows the color spectrum from red to purple as it proceeds from the N to the C terminus. Secondary-structure elements are as follows: β1, residues 3–4; α1, 8–13; α2, 17–29; β2, 32–34; β3, 41–45; β4, 48–56; β5, 60–63; α3, 63–76; β6, 81–84 and β7, 96–101. The orientation of KP4 is identical in (a) and (b). **(c)** Topology diagram of KP4 drawn in a style used in a recent review of α/β folds [31]. The triangles represent β-strands and the circles, α-helices. The smaller elements (i.e. comprising only a few residues) are represented by smaller symbols. Note that the main secondary elements form a topology represented in Figure 9j of [31]. (Parts (a) and (b) created using MolView [55].)

β3–β4 turn without analogous interactions at the β6–β7 turn. It is interesting to note that interleukin-8 (IL-8), a protein with a wide range of immunological effects mediated by interactions at the cell membrane, is a true dimer [42] that looks similar to this toxin. The major differences between IL-8 and KP4 are the connectivity and orientation of the two antiparallel helices with respect to the β-sheet.

Mechanism of KP4 action

As ~80% of the proteins in the α/β-sandwich family function by binding to other proteins (e.g. protein G [34,35], ubiquitin [43] and scorpion toxin [32,33]), it seems likely that KP4 acts by binding to cellular proteins. Regions of the toxin that might be involved in such interactions are suggested by the extremely asymmetric distribution of charge across the toxin surface. When viewed from above the two antiparallel helices (Fig. 4a), the toxin has large patch of positive charge, covering approximately two-thirds of the surface, which surrounds the large protrusion formed by the α3–β4 loop. In contrast, the opposite side of the protein, (the exposed face of the β-sheet) is 'cup'-shaped and covered by hydrophilic residues (Fig. 4b). One possibility is that the β3–β4 loop may be part of the 'active' site of the toxin and that the positive charge in its vicinity allows it to interact with either the phospholipid surface or the putative target membrane protein. The cup itself is covered

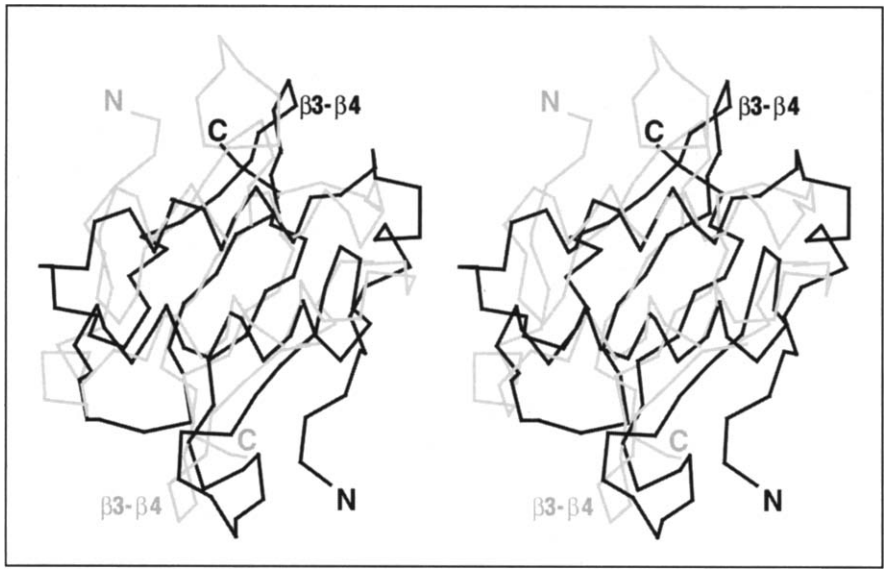

Fig. 3. Stereo diagram demonstrating the internal pseudo-twofold relationship found in KP4. The black lines represent the Cα backbone of KP4 and the gray lines represent the model after rotation about the pseudo-dyad axis. The N and C termini are labeled. For a point of reference, the β3–β4 loop is also labeled. (Figure created using MolView [55].)

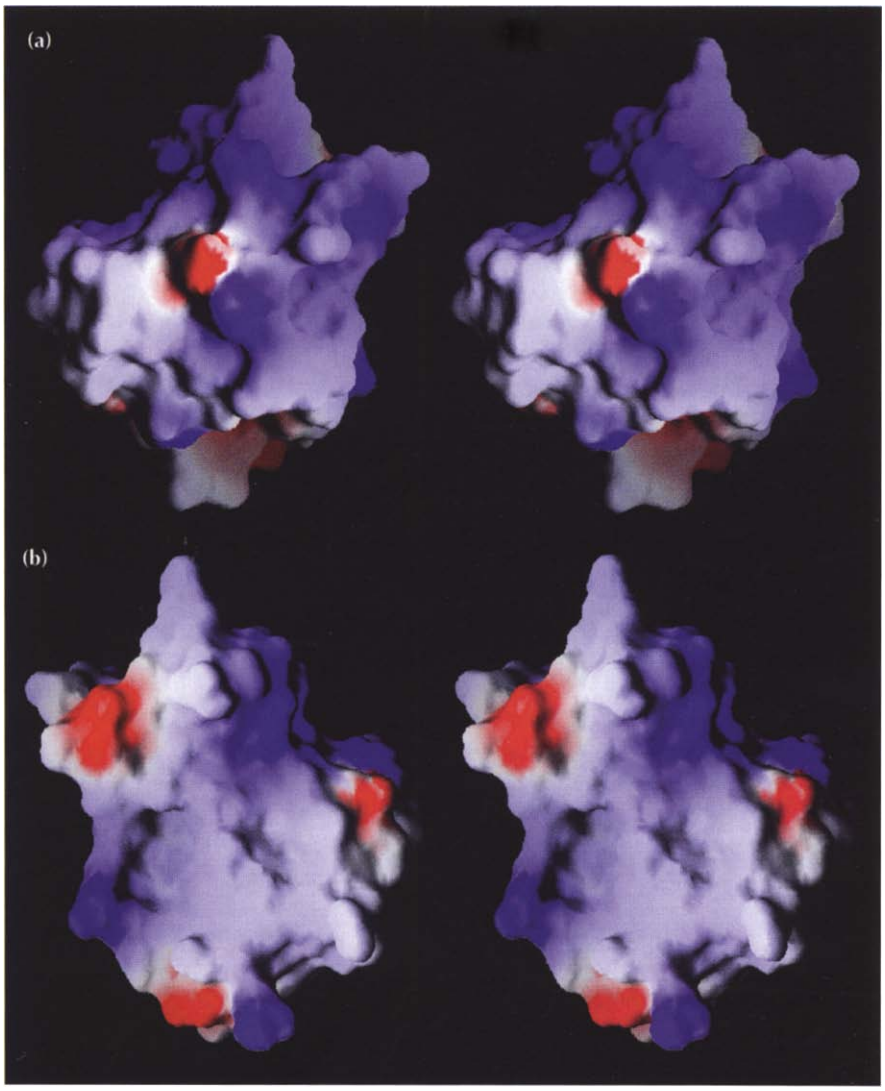

Fig. 4. Stereo diagrams of the KP4 charge potential mapped onto the molecular surface. The positive potential is shown in purple, and the negative potential in red. The β3–β4 protrusion is at the top of the molecule. In **(a)**, the orientation is from above the two α-helices, looking down the pseudo-dyad axis. In **(b)**, KP4 is viewed from the opposite direction to that shown in (a), looking into the exposed β-sheet surface. Note that the large uncharged surface in (b) is composed almost entirely of polar residues. (Figure created using GRASP [56].)

by polar residues and rimmed by several acidic and basic groups. The entire protein is covered by hydrophilic residues, with the exception of a small hydrophobic patch near the N terminus (Fig. 5).

In vivo mechanistic studies

The scorpion toxins are a family of neurotoxins with some interesting, albeit tenuous, similarities to KP4. There are two classes of these single polypeptide chain

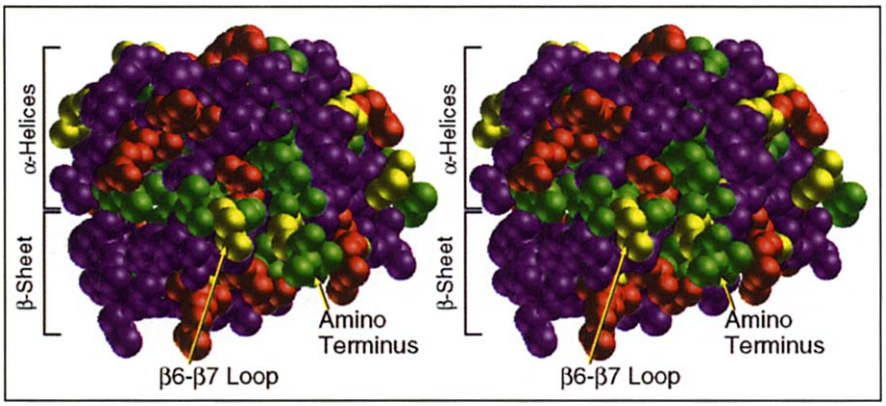

Fig. 5. Stereo space-filling model of KP4 showing the position of the main patch of hydrophobic residues on the surface. In this figure the atoms are represented by solid spheres where charged, polar, glycine, and hydrophobic residues are colored red, blue, yellow, and green, respectively. The view here is approximately parallel to the β-sheet with the α-helices on the top. In this view, the β6–β7 protrusion extends out of the page and the β3–β4 protrusion is occluded from view at the back of the molecule, pointing into the page. (Figure created using MolView [55].)

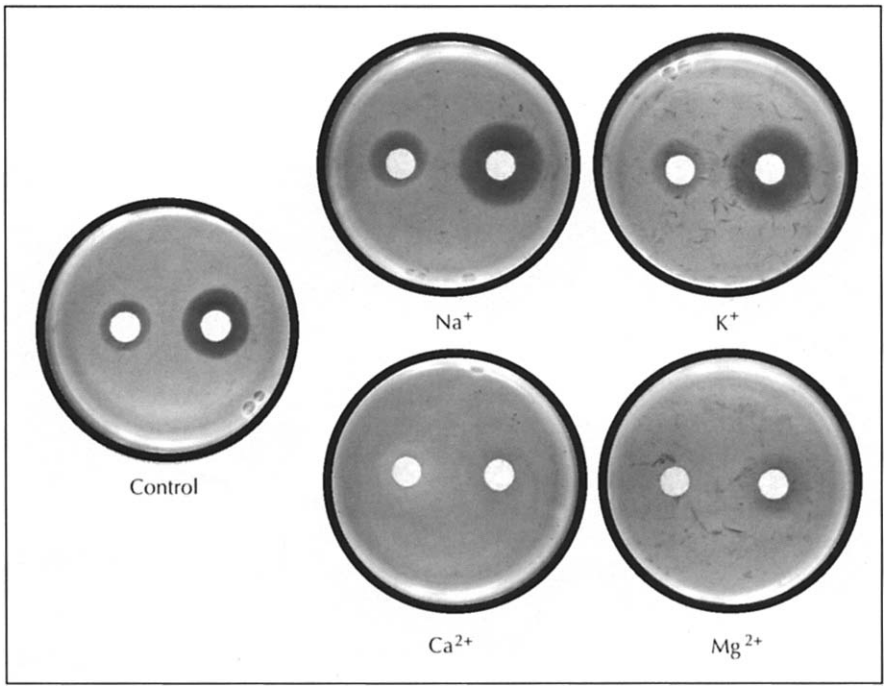

Fig. 6. The effects of cations on KP4 killing. P2 cells were grown in agar containing complete medium [29] with the addition of 0.1 M of one of KCl, NaCl, $MgCl_2$ or $CaCl_2$ and without any additional salts. For each growth condition, two filter blots were placed on top of the agar. The left filter blot contained a ~0.8 μM solution of KP4 and the right filter blot contained a ~8.0 μM solution of KP4. Cell death caused by KP4 is manifest as a clearing about the filter blot after incubation overnight at room temperature.

neurotoxins: short toxins with ~37 amino acids (e.g. charybdotoxin), and long toxins containing ~60–70 amino acids (e.g. *Androctonus australis* Hector II, AaHII). The long neurotoxins, which are of the α/β-sandwich family, can be further subdivided on the basis of their binding characteristics to rat brain synaptosomes and on their electrophysiological effects: the α-toxins (e.g. AaHII) and the β-toxins (e.g. *Centruroides suffusus suffusus* II, CssII). The long toxins exert their neurological effects by acting on Na^+ channels in excitable membranes. Although only about half the size of KP4, the long toxins are similar to KP4 because they are all highly basic proteins stabilized by an extensive network of disulfide bonds. In AaHII, Lys58 is a highly reactive moiety near the C terminus that, upon chemical modification, renders the toxin inactive [44]. The C terminus of AaHII is covalently linked via a disulfide bond to a protrusion formed by the turn between the first α-helix and the first β-strand [33]. An analogous structure is found in KP4. The β3–β4 loop in KP4 has several basic groups along the sides and base of the protrusion (Fig. 4) and is stabilized by a disulfide bond between it and the C-terminal cysteine (Fig. 2). One significant difference between KP4 and AaHII, other than size and topology, is that AaHII has an unusual cluster of four tyrosines on the exposed β-sheet face, whereas KP4 is much more polar at the corresponding face with only a single tyrosine protruding into solvent. It has been suggested that this hydrophobic patch, conserved amongst the long toxins, may play a role in channel binding [32].

In light of this tenuous similarity to the scorpion toxins, KP4 killing efficacy was tested on cells of the P2 strain of *U. maydis* (which are KP4-sensitive) in the presence of additional KCl, NaCl, $MgCl_2$ or $CaCl_2$ (Fig. 6). The addition of up to 0.2 M K^+ and 0.2 M Na^+ did not have a significant effect on KP4 killing, whereas as little as 40 mM Ca^{2+} or 80 mM Mg^{2+} completely rescued P2 cells. It should be noted that growth of P2 cells away from the test area appeared to be equivalent under all test conditions. These results suggest that KP4 inhibits Ca^{2+} channels and that high external Ca^{2+} concentrations rescue the P2 cells by forcing Ca^{2+} through the remaining active channels. The rescue by Mg^{2+} may be due either to competition between KP4 and divalent cation binding or to incomplete Ca^{2+} specificity of the targeted cationic channels.

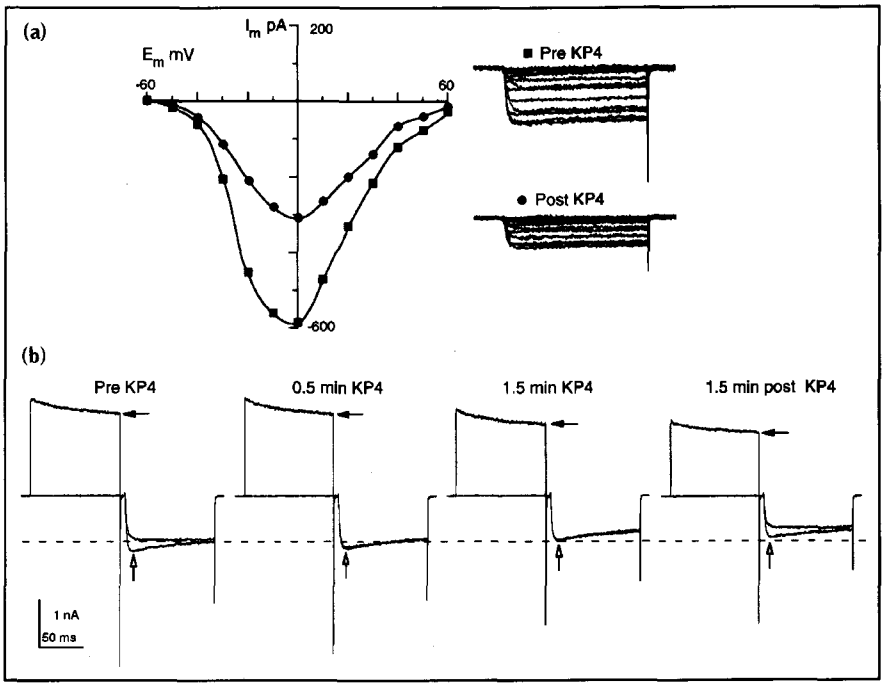

Fig. 7. Modulation of neuronal Ca^{2+} channels by KP4. **(a)** Current–voltage plots (left) and raw current traces (right) show inhibition of voltage-activated Ca^{2+} channel currents in a GH_3 cell after application of ~8 μM KP4. Currents were evoked by 50 ms command steps given from –90 mV, and KP4 was focally applied from a micropipette at a distance of <2 cell diameters. **(b)** In bovine adrenal chromaffin cells, application of a depolarizing prepulse causes Ca^{2+} current facilitation. Pre KP4, a large outward current (filled arrow) is observed during the prepulse (125 mV, 100 ms), and is followed by facilitation (open arrow) of the inward current activated by a step to 0 mV. The starting amplitude of the current evoked at 0 mV in absence of a prepulse is indicated by the dashed line. Scale bars pertain to (b) only.

The results of these rescue experiments strongly suggest that KP4 affects Ca^{2+} channels. Therefore, the effect of KP4 was tested on mammalian neuronal cells for which more is known about the types and kinetics of cationic channels. Standard whole-cell patch clamp techniques were used to examine the effects of KP4 on voltage-activated Na^+, K^+ and Ca^{2+} currents in PC12 (rat pheochromocytoma), GH_3 (rat pituitary tumor) and adrenal chromaffin cells. Focal application of 8.0 μM KP4 for up to 2 min had no effect on activation or inactivation time-courses of Na^+ or K^+ currents, and caused amplitude variations of less than 5% (Na^+ currents, 9 chromaffin cells and 3 PC12 cells; K^+ currents, 5 chromaffin cells and 4 PC12 cells). KP4 did, however, modulate Ca^{2+} currents. In GH_3 cells, KP4 at 0.8 μM and 8.0 μM inhibited high-threshold voltage-activated Ca^{2+} current [45] by an average of 30±5% (n=3) and 48±2% (n=7), respectively (Fig. 7a).

In chromaffin cells, KP4 application caused an initial enhancement of current similar to that observed in response to a depolarizing prepulse [46] (Fig. 7b). Indeed, in the presence of KP4 (0.5 min KP4, approximate concentration 0.8 μM) this current appears identical to the facilitated current, that is KP4 mimics prepulse facilitation. This effect persists with continued application of KP4 (1.5 min KP4), but is overlaid on a more slowly developing inhibition of steady-state current. The facilitatory effect of KP4 reverses with removal of the peptide, but the steady-state inhibition persists (1.5 min post KP4). Similar results were observed in PC12 cells.

With continued application of KP4 (8 μM), steady-state current amplitude was decreased by an average of 28±3% in chromaffin cells (n=5), and 25±5% in PC12 cells (n=7). In these mammalian neuronal cells, therefore, the prevalent action of KP4 is inhibition of voltage-activated Ca^{2+} channel currents. As mammalian cells do not contain Mg^{2+} channels, the Mg^{2+}-dependent rescue of P2 fungal cells cannot be analyzed.

Biological implications

A number of strains of fungi, termed 'killer' strains, have an unusual symbiotic relationship with the double-stranded (ds) RNA viruses that persistently infect them. Unlike the non-fungal viruses, these dsRNA viruses are not released by the host fungus during the normal viral life cycle and are therefore dependent upon host survival for viral replication. To lend the host strain a selective advantage over the other strains of fungi, the viruses encode small toxins that kill the competitive fungal strains but not the host strain. Most of the toxins from *Ustilago maydis* (corn smut) and *Saccharomyces cerevisiae* (yeast) appear to act by recognizing the target cells and then disrupting the membrane integrity.

The structure of the fungal toxin expressed by the P4 strain of *U. maydis* (KP4) was determined to try to ascertain its mechanism of action, its evolutionary origins, and as a source of potential new leads for anti-fungal agents. KP4, a 105-residue polypeptide, was found to be a tightly packed, stable protein with a novel topology. Its stability and the extremely hydrophilic nature of its surface make it very unlikely that KP4 kills cells by forming ion channels in their membranes, a mechanism that has been proposed for other killer toxins. Similarities between a highly basic protrusion from the main β-sheet of KP4 and the active site of scorpion toxins, which bind to (and alter) cation channels on excitable membranes, led to experiments

demonstrating that KP4-sensitive cells can be rescued by the addition of Ca^{2+} or Mg^{2+} but not Na^+ or K^+. This suggested that KP4 kills target fungal cells by blocking divalent cation channels. This hypothesis was substantiated by experiments on several types of mammalian neuronal cells, in which marked inhibition of voltage-gated Ca^{2+} channels was detected.

The effects of KP4 on mammalian Ca^{2+} channels, in conjunction with the fungal rescue experiments, strongly support the hypothesis that KP4 affects target fungal cells via Ca^{2+} (and/or possible Mg^{2+}) channels. As Ca^{2+} plays such a major role in cell growth and regulation, it is conceivable that KP4 was originally expressed by the virus to amplify virus production by controlling host replication. Perhaps the most surprising result is that fungal and mammalian Ca^{2+} channels are conserved to such a degree that both appear to be affected by the same protein inhibitor. In addition, these findings suggest that Ca^{2+} channel blockers might serve as lead compounds for new anti-fungal agents against human pathogens (e.g. *Pneumocystis carinii* and *Chlymydia*). Studies are underway to define the recognition sites on the toxin using site-directed mutagenesis, and to examine the physiological effects of the toxin on mammals, the effects of KP4 on the ultrastructure of target cells, and the pharmacological details of the toxin action on the Ca^{2+} channels.

Materials and methods

KP4 purification and crystallization

KP4 was purified from *U. maydis* P4 cell culture as previously described [30]. In brief, the toxin was isolated from the supernatant of the P4 strain of *U. maydis* grown in complete medium (1% dextrose, 2.5% bactocasitone, 0.1% yeast extract, and 0.15% ammonium nitrate) for 3–7 days at 25°C under extensive aeration. The supernatant was stirred overnight with CM Sephadex C-25 beads (Pharmacia, Piscataway, NJ) in 25 mM sodium acetate, pH 5.5 at 4°C. The toxin was then eluted using the same buffer with the addition of 1 M NaCl. The eluent was then dialyzed against water and purified using the high-resolution cation-exchange chromatography matrix, Mono-S™ (Pharmacia), attached to an FPLC™ (Pharmacia) system using 50 mM 2-[*N*-morpholino]ethanesulfonic acid at pH 6.0 and eluted with ~0.1 M NaCl in the same buffer. The toxin was then finally purified using the size-exclusion chromatography matrix, Superdex 75™ (Pharmacia).

The previously described hexagonal crystal form [30] did not diffract X-rays beyond 2.8 Å resolution and was found to be difficult to derivatize. A new crystal form was found using the hanging drop method at room temperature where the reservoir contained 0.2 M sodium citrate, 20% isopropanol in 0.1 M HEPES buffer pH 7.5. The drop contained 5 µl of ~10 mg ml^{-1} KP4 toxin in water, and 5 µl of the reservoir solution. These crystals yielded higher resolution data (to 1.7 Å resolution using conventional X-ray sources and beyond 1.4 Å at the Cornell High Energy Synchrotron Source) and were used in heavy-atom derivative searches.

Data collection, processing and reduction

All data were collected at 4°C using an R-axis imaging detector and a Rigaku X-ray generator. The diffraction images were indexed and integrated using the program DENZO [47]. Entire data sets were collected from single crystals and scaled using SCALEPACK [47]. The final native data set was >90% complete to 1.9 Å resolution, with an R_{sym} of 12.3% in the highest resolution bin, and a redundancy of observations of ~3.4.

The new crystal form belongs to the $P2_1$ space group. From V_m calculations, it was apparent that there were probably two toxin molecules in the asymmetric unit. This was confirmed by a large peak in the κ=180° self-rotation function. This peak had a height of 6σ which was 0.35 the height of the origin peak and three times the value of the next highest peak. The position of this dyad axis was determined from the heavy-atom derivative positions.

Phase determination

Of the 19 different heavy-atom compounds tested, the only usable derivative was gold potassium cyanide [$KAu(CN)_2$]. A stock solution of the gold derivative was prepared by dissolving it to saturation in the reservoir solution. This solution was then added directly to the hanging drop (final dilution of ~1:5) and allowed to react for 7–9 days. Two derivative crystal data sets were collected, combined, and scaled to native data using SCALEIT in the CCP4 program suite [48]. Two gold-binding sites were identified on a difference Patterson map and the positions refined by MLPHARE [49]. Using phases calculated from these two sites, two additional sites were found in a difference Fourier (F_{PH}–F_P) electron-density map. These four heavy-atom sites were then refined including anomalous dispersion signals. The final figure of merit was 0.45 and the phasing power was 1.46 to 2.5 Å resolution. The twofold axis, determined by the self-rotation function, accurately related one pair of heavy-atom sites to the other pair. This positioned the non-crystallographic dyad axis relative to the heavy-atom positions.

An electron-density map was calculated to 2.8 Å using the single isomorphous replacement (SIR) phases. To generate a molecular mask, this map was solvent-flattened by density modification (DM) in the CCP4 program package [48]. The map exhibited clear protein–solvent boundaries and maintained the non-crystallographic twofold symmetry. MAPMAN (part of the 'O' graphics package [41]) was then applied to the SIR map to create a crude protein skeleton that was then edited using 'O' [41]. A mask for twofold averaging was calculated from this skeleton using the programs ATOMASK and MASK [50].

MAPMODIFY (J Tesmer, personal communication) was then used to improve the phases by solvent flattening and real-space averaging. The protein electron-density map was first calculated to 5 Å, the density outside the mask flattened as solvent, and the density inside the mask averaged according to the non-crystallographic twofold axis. The phases were then slowly extended from 5 Å to 2.8 Å in step sizes equal to half of the smallest reciprocal unit cell dimension. For each step, eight cycles of solvent flattening, molecular twofold averaging, and phase combination or weighting were performed. Phase combination was used in the first two cycles, whereas the remaining six cycles used the calculated phases after weighting using SIGMAA [51].

At this stage, the major secondary structural elements were clearly visible in the 2.8 Å electron-density map. A partial polyalanine model was built using 'O' [41] on an ESV graphics workstation. While almost all of the connections between the

secondary structural elements were ambiguous, the quality of the map was sufficient to easily determine the polarity of the two α-helices and the positions (but not identity) of 88 out of the total 105 residues. This partial polyalanine model was then energy-minimized against the data using the Powell conjugate-gradient minimization in X-PLOR [52]. At this time, because the center of mass of two models were refined independently, it became clear that the position of the non-crystallographic twofold axis was displaced by 0.45 Å in the X–Z plane. Subsequent averaging used this new dyad position. Calculated phases from this partial model were then combined with the SIR phases and a new, twofold averaged, map was calculated to 2.8 Å. As it became apparent that some loops were not included in the initial mask, the mask was updated and the map recalculated. At this point, the electron density and connectivity was of sufficient quality to unambiguously assign all of the 105 residues in both copies of KP4 in the asymmetric unit. The resolution was extended from 2.8 Å to 1.9 Å as the model was refined using several cycles of the simulated annealing protocol in X-PLOR followed by manual rebuilding using 'O' [41]. During refinement, unaveraged $2F_o–F_c$ electron-density maps were calculated using model phases. The overall geometry was examined and problematic areas were identified using the program PROCHECK (version 3.0) [53]. The non-crystallographic twofold axis was not enforced during refinement, yet the two molecules are almost identical with an rms deviation of 0.249 Å between corresponding Cα positions. The current model contains all 105 residues for each molecule with an additional 109 water molecules in the asymmetric unit. The only outliers in the Ramachandran plots are glycine residues and all geometrical parameters examined by PROCHECK [53] are either well within or better than the range of values expected for a protein structure determined to this resolution.

Effects of KP4 on mammalian Ca^{2+} channels

Ca^{2+} channel current records were obtained by standard whole-cell patch clamp methods. Current signals from an Axopatch 200A amplifier were filtered at 5 kHz, digitized at 10 kHz, and subjected to P/4 leak subtraction, acquired and analyzed with Pulse (Instrutech Corp., Great Neck, NY) software. Cells were held at −90 mV and command steps were applied every 5 s. Ca^{2+} current amplitudes typically increased within the first few minutes of achieving whole-cell access, and then remained stable for tens of minutes. The bath solution contained (in mM) 135 tetraethylammonium (TEA)-Cl, 4 KCl, 10 $BaCl_2$, 1 $MgCl_2$, 10 HEPES and 1 μM tetrodotoxin (TTX). The patch pipette solution contained (in mM) 150 CsCl, 2 Mg-ATP, 0.5 GTP, 2 5-bis-[*o*-aminophenoxy]ethane-N,N,N′,N′-tetraacetic acid (BAPTA) and 10 HEPES (pH 7.3). As noted in the text, KP4 was also tested against voltage-activated Na^+ and K^+ currents. For sodium currents the same patch pipette solution was used but the bath solution contained (in mM) 138 NaCl, 9 KCl, 1 $CaCl_2$, 1 $MgCl_2$, 10 TEA-Cl, 10 HEPES and 0.25 $CdCl_2$. For K^+ current recordings the bath solution contained (in mM) 143 NaCl, 4 KCl, 1 $CaCl_2$, 1 $MgCl_2$, 10 HEPES, 0.25 $CdCl_2$ and 1 μM TTX and the patch pipette solution contained (in mM) 150 KCl, 1 $MgCl_2$, 5 BAPTA and 10 HEPES. GH_3 cells were a generous gift from Dr L Yu (Indiana University Medical School), adrenal chromaffin cells were obtained by standard dissection and collagenase procedures, and PC12 cells were from the American Type Culture Collection.

The coordinates and structure factors have been deposited in the Brookhaven Protein Data Bank with entry codes 1KPT and R1KPTSF, respectively.

Acknowledgements: We would like to thank Ms Tiffany Sullivan for producing some of the KP4 used in this study. This work was supported by grants from the National Institutes of Health (GM10704 to TJS, R01GM43462 to SR, and GM422182 to WFF), from the Lucille P Markey Charitable Trust (Purdue Structural Biology Center), the American Heart Association to SR, the Indiana Affiliate Grant to SR, the Indiana State Faculty Research Grant to RJB, the ΣXi Research Society to AK, and the Indiana Academy of Science to AK.

References

1. Bevan, E.A. & Mankower, M. (1963). The physiological basis of the killer character in yeast. *Proc. Int. Congr. Genet.* **XI**, 1202–1203.
2. Wood, H.A. & Bozarth., R.F. (1973). Heterokaryon transfer of virus-like particles and a cytoplasmically inherited determinant in *Ustilago maydis*. *Phytopathology* **63**, 1019–1021.
3. Bozarth, R.F., *et al.*, & Steinlauf, R. (1981). The molecular weight and packaging of dsRNAs in the mycovirus from *Ustilago maydis* killer strains. *Virology* **113**, 492–502.
4. Esteban, R. & Wickner, R.B. (1986). Three different M1 RNA-containing virus-like particle types in *Saccharomyces cerevisiae*: *in vitro* M1 double stranded RNA synthesis. *Mol. Cell. Biol.* **6**, 1552–1561.
5. Fujimura, T., Ribas, J.C., Makhov, A.M. & Wickner, R.B. (1992). Pol of *gag–pol* fusion protein required for encapsidation of viral RNA of yeast L-A virus. *Nature* **359**, 746–749.
6. Cheng, R.H., *et al.*, & Steven, A.C. (1994). Fungal virus capsids: cytoplasmic compartments for the replication of double-stranded RNA formed as icosahedral shells of asymmetric *gag* dimers. *J. Mol. Biol.* **244**, 255–258.
7. Caspar, D.L.D. & Klug, A. (1962). Physical principles in the construction of regular viruses. *Cold Spring Harb. Symp. Quant. Biol.* **27**, 1–24.
8. Young, T.W. & Yagiu, M. (1978). A comparison of the killer character in different yeasts and its classification. *Antonie van Leeuwenhoek* **44**, 59–77.
9. Bussey, H., Saville, D., Greene, D.J. & Bostian, K.A. (1983). Secretion of *Saccharomyces cerevisiae* killer toxin: processing of the glycosylated precursor. *Mol. Cell Biol.* **3**, 1362–1370.
10. Bostian, K.A., *et al.*, & Tipper, D.J. (1984). Sequence of the preprotoxin dsRNA gene of type 1 killer yeast: multiple processing produces a two component toxin. *Cell* **36**, 741–751.
11. Dimochowska, A., Dignard, D., Henning, D., Thomas, D.Y. & Bussey, H. (1987). Yeast KEX1 gene encodes a putative protease with a carboxypeptidase B-like function involved in the killer toxin and a-factor precursor processing. *Cell* **50**, 573–584.
12. Bussey, H., *et al.*, & Thomas, D.Y. (1990). Genetic and molecular approaches to synthesis and action of the yeast killer toxin. *Experientia* **46**, 193–200.
13. Tipper, D.J. & Bostian, K.A. (1984). Double-stranded ribonucleic acid killer systems in yeast. *Microbiol. Rev.* **48**, 125–156.
14. Middelbeek, E.J., *et al.*, & Vogels, G.D. (1980). Physiological conditions affecting the stability of *Saccharomyces cerevisiae* killer toxin and energy requirement for toxin action. *Antonie van Leeuwenhoek* **46**, 483–497.
15. Bussey, H. (1981). Physiology of killer factor in yeast. *Adv. Microb. Physiol.* **22**, 93–122.
16. De La Pena, P., Barros, F., Gascon, S., Lazo, P.S. & Ramos, S. (1981). Effect of yeast killer toxin on sensitive cells of *Saccharomyces cerevisiae*. *J. Biol. Chem.* **256**, 10420–10425.
17. Martinac, B., *et al.*, & Kung, C. (1990). Yeast K1 killer toxin forms ion channels in sensitive yeast spheroplasts and in artificial liposomes. *Proc. Natl. Acad. Sci. USA* **87**, 6228–6232.
18. Kagan, B. (1983). Mode of action of yeast killer toxins: channel formation in lipid bilayer membranes. *Nature* **302**, 709–711.
19. Puhalla, J.E. (1968). Compatibility reactions on solid medium and interstrain inhibition in *Ustilago maydis*. *Genetics* **60**, 461–474.
20. Koltin, Y. & Day, P.R. (1975). Specificity of *Ustilago maydis* killer proteins. *Appl. Microbiol.* **30**, 694–696.
21. Koltin, Y. (1988). The killer system of *Ustilago maydis*: secreted polypeptides encoded by viruses. In *Viruses of Fungi and Simple Eukaryotes*. (Koltin, Y. & Leibowitz, M., eds), pp. 209–242, Marcel Dekker, New York.
22. Peery, T., Shabat-Brand, T., Steinlauf, R., Koltin, Y. & Bruenn, J. (1987). The virus encoded toxin of *Ustilago maydis* — two polypeptides are essential for activity. *Mol. Cell. Biol.* **7**, 470–477.
23. Steinlauf, R., Peery, T., Koltin, Y. & Bruenn, J. (1988). The *Ustilago maydis* virus encoded toxin — effect of KP6 on cells and spheroplasts. *Exp. Mycol.* **12**, 264–274.

24. Tao, J., *et al.*, & Bruenn, J.A. (1990). *Ustilago maydis* KP6 toxin: structure, expression in *Saccharomyces cerevisiae*, and relationship to other cellular toxins. *Mol. Cell. Biol.* **10**, 1373–1381.
25. Zizi, M., Finkler, A. & Koltin, Y. (1995). Association of both subunits of *Ustilago maydis* toxin, KP6, forms large voltage-independent channels. *Biophys. J.* **68**, A203.
26. Duax, W.L., *et al.*, & Straubinger, R. (1995). Crystallization of the a polypeptide of the KP6 killer toxin. *Biophys. J.* **68**, A203.
27. Bussey, H. (1972). Effects of yeast killer factor on sensitive cells. *Nat. New Biology* **235**, 73–75.
28. Levine, R., Koltin, Y. & Kandel, J. (1979). Nuclease activity associated with the *Ustilago maydis* virus induced killer proteins. *Nucleic Acids Res.* **6**, 3717–3732.
29. Ganesa, C., Chang, Y.-H., Flurkey, W.H. & Bozarth, R.F. (1989). Purification and molecular properties of the toxin coded by *Ustilago maydis* virus P4. *Biochem. Biophys. Res. Commun.* **162**, 651–657.
30. Gu, F., *et al.*, & Smith, T.J. (1994). The characterization and crystallization of a virally encoded *Ustilago maydis* KP4 toxin. *J. Mol. Biol.* **243**, 792–795.
31. Orengo, C.A. & Thornton, J.M. (1993). Alpha plus beta folds revisited: some favoured motifs. *Structure* **1**, 105–120.
32. Fontecilla-Camps, J.C., *et al.*, & Bugg, C.E. (1981). Architecture of scorpion neurotoxins: a class of membrane-binding proteins. *Trends Biochem. Sci.* **6**, 291–296.
33. Housset, D., Habersetzer-Rochat, C., Astier, J.-P. & Fontecilla-Camps, J.C. (1994). Crystal structure of toxin II from scorpion *Androctonus australis* Hector refined at 1.3 Å resolution. *J. Mol. Biol.* **238**, 88–104.
34. Derrick, J.P. & Wigley, D.B. (1992). Crystal structure of a streptococcal protein G domain bound to an Fab fragment. *Nature* **359**, 752–754.
35. Achari, A., *et al.*, & Whitlow, M. (1992). 1.67 Å X-ray structure of the B2 immunoglobulin domain of streptococcal protein G and comparison to the NMR structure of the B1 domain. *Biochemistry* **31**, 10449–10457.
36. Nonaka, T., Mitsui, Y., Irie, M., & Nakamura, K.T. (1991). Three-dimensional structure of ribonuclease Ms *3'-guanylic acid complex at 2.5 Å resolution. *FEBS Lett.* **283**, 207–209.
37. Sevcik, J., Dodson, E.J. & Dodson, G.G. (1991). Determination and restrained least-squares refinement of the structures of ribonuclease Sa and its complex with 3'-guanylic acid at 1.8 Å resolution. *Acta Crystallogr. B* **47**, 240–253.
38. Lenz, A., Heinemann, U., Maslowska, M. & Saenger, W. (1991). X-ray analysis of cubic crystals of the complex formed between ribonuclease T1 and guanosine-3',5'-bisphosphate. *Acta Crystallogr. B* **47**, 521–527.
39. Nakai, T., Yoshikawa, W., Nakamura, H. & Yoshida, H. (1992). The three-dimensional structure of guanine-specific ribonuclease F1 in solution determined by NMR spectroscopy and distance geometry. *Eur. J. Biochem.* **208**, 41–51.
40. Rico, M., *et al.*, & Nieto, J.L. (1991). 3D structure of bovine pancreatic ribonuclease A in aqueous solution: an approach to tertiary structure determination from a small basis of ^{1}H NMR NOE correlations. *J. Biomol. NMR* **1**, 283–298.
41. Jones, T.A., Zou, J.-Y., Cowan, S.W. & Kjeldgaard, M. (1991). Improved methods for building protein models in electron density maps and the location of errors in these models. *Acta Crystallogr. A* **47**, 110–119.
42. Baldwin, E.T., *et al.*, & Wlodawer, A. (1991). Crystal structure of interleukin 8: symbiosis of NMR and crystallography. *Proc. Natl. Acad. Sci. USA* **88**, 502–506.
43. Vijay-Kumar, S., *et al.*, & Cook, W.J. (1987). Comparison of the three-dimensional structures of human, yeast, and oat ubiquitin. *J. Biol. Chem.* **262**, 6396–6399.
44. Sampieri, F. & Habersetzer-Rochat, C. (1978). Structure–function relationships in scorpion neurotoxins: identification of the super-reactive lysine in toxin I of *Androctonus australis* Hector. *Biochim. Biophys. Acta* **535**, 100–109.
45. Matteson, D.R. & Armstrong, C.M. (1986). Properties of two types of calcium channels in clonal pituitary cells. *J. Gen. Physiol.* **87**, 161–182.
46. Artalejo, C.R., Mogul, D.J., Perlman, R.L. & Fox, A.P. (1991). Three types of bovine chromaffin cell Ca^{2+} channels: facilitation increases the opening probability of a 27 pS channel. *J. Physiol.* **444**, 213–240.
47. Otwinoski, Z. (1993). DENZO. In *Data Collection and Processing.* (Sawyer, L. Isaacs, N. and Bailey, S., eds), pp. 56–62, SERC Daresbury Laboratory, Warrington, UK.
48. Beiley, S. (1994). The CCP4 suite: programs for protein crystallography. *Acta Crystallogr. D* **50**, 760–763.
49. Otwinowski, Z. (1991). Maximum likelihood refinement of heavy atom parameters. In *Isomorphous Replacement and Anomalous Scattering: Proceedings of the CCP4 study weekend 25–26 January 1991.* (Wolf, W., Evans, P.R. & Leslie, A.G.W., eds), pp. 80–86, SERC Daresbury Laboratory, Warrington, UK.
50. Bolin, J.T., Smith, J.L. & Muchmore, S.W. (1993). Considerations in phase refinement and extension: experiments with a rapid and automatic procedure. In *Proceedings of the American Crystallographic Association Meeting*, Albuquerque, NM. Vol. **21**, p. 51.
51. Read, R.J. (1986). Improved Fourier coefficients for maps using phases from partial structures with errors. *Acta Crystallogr. A* **42**, 140–149.
52. Brünger, A.T. (1992). *X-PLOR (Version 3.1), User's Guide.* Yale University, New Haven, CT.
53. Laskowski, R.A., MacArthur, M.W., Moss, D.S. & Thornton, J.M. (1993). PROCHECK: a program to check the stereochemical quality of protein structures. *J. Appl. Crystallogr.* **26**, 283–291.
54. Brünger, A.T. (1991). Simulated annealing in crystallography. *Annu. Rev. Phys. Chem.* **42**, 197–233.
55. Smith, T.J. (1995). MolView: a program to analyze and display atomic structures on the Macintosh personal computer. *J. Mol. Graphics* **13**, 122–125.
56. Nicholls, A. (1993). *GRASP: Graphical Representation and Analysis of Surface Properties.* Columbia University, New York.

Received: **26 May 1995**; revisions requested: **22 Jun 1995**; revisions received: **29 Jun 1995**. Accepted: 7 **Jul 1995**.